Atmospheric radiocarbon measurements to quantify CO_2 emissions in the UK from 2014 to 2015

Angelina Wenger[1], Katherine Pugsley[1], Simon O'Doherty[1*], Matt Rigby[1], Alistair J. Manning[1,2], Mark Lunt[3], Emily White[1]

[1]School of Chemistry, University of Bristol, Bristol, BS8 1TS, UK
[2]Met Office, Exeter, Devon, EX1 3PB, UK
[3]School of Geosciences, University of Edinburgh, UK
*Correspondence to: Angelina Wenger (aw12579@my.bristol.ac.uk), Simon O'Doherty (s.odoherty@bristol.ac.uk)

Abstract. We present $\Delta^{14}CO_2$ observations and related greenhouse gas measurements at a background site in Ireland and a tall-tower site in the east of the UK that is more strongly influenced by fossil fuel sources. These observations have been used to calculate the contribution of fossil fuel sources to the atmospheric CO_2 mole fractions; this can be done, as emissions from fossil fuels do not contain $^{14}CO_2$ and cause a depletion in the observed $\Delta^{14}CO_2$ value. The observations are compared to simulated values. Two corrections need to be applied to radiocarbon-derived fossil fuel CO_2 ($ffCO_2$), one for pure $^{14}CO_2$ emissions from nuclear industry sites and one for a disequilibrium of the isotopic signature of older biospheric emissions (heterotrophic respiration) and CO_2 in the atmosphere. Measurements at both sites were found to only be marginally affected by $^{14}CO_2$ emissions from nuclear sites. Over the study period of 2014 – 2015, the biospheric correction and the correction for nuclear $^{14}CO_2$ emissions were similar, at 0.34 and 0.25 ppm $ffCO_2$ equivalent, respectively. The observed $ffCO_2$ at the site was not significantly different from simulated values based on the EDGAR 2010 bottom-up inventory. We explored the use of high-frequency CO observations as a tracer of $ffCO_2$, by deriving a constant ratio of CO enhancements to $ffCO_2$ ratio for the mix of UK fossil fuel sources. This ratio was found to be 5.7 ppb ppm^{-1}, close to the value predicted using inventories and the atmospheric model of 5.1 ppb ppm^{-1}. The site in the east of the UK was strategically chosen to be some distance from pollution sources so as to allow for the observation of well-integrated air masses. However, this, and the large measurement uncertainty in $^{14}CO_2$, lead to a large overall uncertainty in the $ffCO_2$, being around 1.8 ppm compared to typical enhancements of 2 ppm.

1 Introduction

The level of carbon dioxide (CO_2) in the atmosphere is rising because of anthropogenic emissions, leading to a change in climate (IPCC, 2014; Le Quéré et al., 2018). Robust quantification of anthropogenic fossil fuel CO_2 ($ffCO_2$) emissions is vital for understanding the global and regional carbon budgets. However, biospheric fluxes are typically an order of magnitude larger than anthropogenic emissions (Le Quéré et al., 2018), which makes it difficult to utilise CO_2 observations in a "top-down" approach to estimate $ffCO_2$ emissions (Nisbet and Weiss, 2010). For this reason, most $ffCO_2$ emission estimates use bottom-up methods, based on inventories and process models (Gurney et al., 2017; van Vuuren et al., 2009; Zhao et al., 2012). These methods take into consideration factors such as the reported energy usage, the carbon content of the fuel and oxidation ratios (BEIS, 2018; Friedlingstein et al., 2010; Le Quéré et al., 2016). While these CO_2 emission inventories are considered to be reasonably accurate, the quality of them is dependent on the statistics and reporting methods. In high income countries, uncertainties are estimated to be around 5 %, whereas, in low-middle income countries, these uncertainties can exceed 10 % (Ballantyne et al., 2015). However, distributing these emissions in space and time adds additional uncertainty, potentially leading to uncertainties on the order of 50 % (Ciais et al., 2010). According to bottom-up estimates in the UK in 2016, CO_2 emissions accounted for 81 % of all of the UK's greenhouse gas emissions (BEIS, 2018).

Unstable isotope measurements can provide a way to disentangle different sources, and directly quantify $ffCO_2$. Radiocarbon (^{14}C, half-life 5700±30 years (Roberts and Southon, 2007)) is produced in the stratosphere and subsequently oxidised to CO_2 (Currie, 2004). It is integrated into other carbon pools that have a relatively fast carbon exchange with the atmosphere, such as the biosphere and the surface ocean. Fossil fuels, having been isolated from the atmosphere for millions of years, are completely depleted in ^{14}C. Burning fossil fuels, therefore, causes a depletion in $^{14}CO_2$ that can be observed in the atmosphere, a phenomenon known as the Suess effect (Suess, 1955). Previously, $^{14}CO_2$ has been used to estimate CO_2 from fossil fuel burning ($ffCO_2$) in, among other places, the USA, Canada, New Zealand as well as some European countries (Bozhinova et al., 2016; Graven et al., 2012; Levin et al., 2003; Miller et al., 2012; Turnbull et al., 2009a; Vogel et al., 2013; Xueref-Remy et al., 2018). However, it has not yet been used in the UK, partly because it was thought that the relatively high density of nuclear power plants emitting pure $^{14}CO_2$ would mask the depletion from fossil fuel burning. Previous studies suggest that this masking effect is particularly strong in the UK as the most prevalent type of nuclear power plant, Advanced Gas Reactors (AGR), have comparatively high $^{14}CO_2$ emissions (Bozhinova et al., 2016; Graven and Gruber, 2011). In previous studies, parametrized ^{14}C emissions were used, calculated by relating the power production of a nuclear power plant with a plant-type-specific emission factor. However, Vogel et al., 2013 showed that 14-day integrated atmospheric $^{14}CO_2$ observations in a region of Canada with high nuclear $^{14}CO_2$ emissions, could be better simulated using the reported monthly emissions from nuclear power plants, instead of the parameterized values. Reported emissions are likely better than parameterized values, as $^{14}CO_2$ emission from nuclear power plants can vary depending on operational parameters as well as the presence of fuel or cooling agent impurities.

Although $^{14}CO_2$ is an important tracer for fossil fuel CO_2 emissions, measurements are sparse. This is primarily because of the cost and time required per sample. This has motivated researchers to combine $^{14}CO_2$ observations with other tracers, such as carbon monoxide (CO) to improve temporal coverage (Gamnitzer et al., 2006; Levin and Karstens, 2007; Lopez et al., 2013; Miller et al., 2012; Turnbull et al., 2006, 2011). For example, high-frequency CO data have been used with $^{14}CO_2$ measurements to regularly calibrate the CO_{enh} (enhancement of CO from background concentration) to $ffCO_2$ ratio, based on weekly ^{14}C measurements in Europe (Berhanu et al., 2017; Levin and Karstens, 2007). However, using a CO_{enh}: $ffCO_2$ ratio to estimate higher frequency $ffCO_2$ can be challenging to implement even when using a well-calibrated ratio because the ratios of different sources and sinks impacting each measurement can vary considerably, as each source emits with its own CO : $ffCO_2$ ratio (Adams et al., 2016).

As part of the Greenhouse gAs Uk and Global Emissions (GAUGE) network (Palmer et al., 2018), weekly $^{14}CO_2$ measurements have been made at two sites between July 2014 and November 2015: Tacolneston, Norfolk (TAC, 52.51°N, 1.13°E), a site that is influenced by anthropogenic sources in England and Mace Head, Ireland (MHD, 53.32°N, -9.90°E), a background site. In this work, we present a way to model the isotopic composition at TAC and MHD and compare the modelled data to the observations. The $^{14}CO_2$ measurements are then used to calculate $ffCO_2$ at TAC. The need for this radiocarbon-based calculation of the $ffCO_2$ to be corrected for the influence of $^{14}CO_2$ from nuclear power plants and the biospheric disequilibrium is also discussed. As an attempt to improve the temporal resolution of the $ffCO_2$ we define the CO_{enh}: $ffCO_2$ ratios at TAC and explore the potential for calculating $ffCO_2$ from high frequency CO observations.

2 Measurements

2.1 Site setup

The TAC tall tower measurement site was set up in 2012 as part of the UK DECC (Deriving Emissions linked to Climate Change) network (Figure 1). It is operated by Bristol University and the University of East Anglia. More details on the site and the network have been previously published (Stanley et al., 2018). The site is located in Norfolk, approximately 140 km north east of London. It was thought to be the most appropriate site in the UK DECC tall tower network for characterising $ffCO_2$ emissions from the UK using $^{14}CO_2$ because it has the most influence from fossil fuel sources and the least influence from nuclear power stations. The TAC tower site has 3 inlet heights; 54 m, 100 m and 185 m. CO is observed from the 100 m inlet once every 20 minutes. The CO_2 observations are reported as 1 minute means and all heights were sampled at an interval of 20 minutes per height. The highest height (185 m) was used for the $^{14}CO_2$ measurements as it was assumed that it would be the most representative for well-integrated air masses. A background observation is necessary for the $^{14}CO_2$ method, to evaluate the relative depletion caused by recently added emissions of $ffCO_2$. Different types of sites have been utilised as background in previous studies: relatively unpolluted sites upwind of significant fossil CO_2 sources (Lopez et al., 2013), high altitude observations (Bozhinova et al., 2014; Levin and Kromer, 1997), free troposphere observations from an aircraft (Miller et al., 2012; Turnbull et al., 2011) and a mildly polluted site upwind of the polluted site (Turnbull et al., 2015). MHD, located on the west coast of Ireland, was used as the background site for this study and weekly sampling was performed when air masses were representative of clean air coming from the Atlantic (Figure 1). This study utilised both flask and, for some species, high-frequency *in situ* data from two sites (MHD and TAC), Table 1 gives an overview of the measurement techniques used, the calibration scales and the operator of the specific instrument or method. For CO, the flask and the *in situ* data were reported on different calibration scales. Comparisons of co-located observations in MHD show that there is a significant difference between the two scales (supplementary material S1). Conversion between the CSIRO-98 and the WMO-2014 CO scale is non-trivial as there is a time and concentration dependent difference between the two scales and no published conversion method is yet available. It was decided that only the *in situ* data would be utilised for the CO ratio analysis, to avoid any effect these calibration scale differences might have on the CO ratio analysis. At TAC the *in situ* CO observations (100m) were made at a different height to the flask sampling (185m). Observations of CH_4 and CO_2 at the two heights were similar (less than 0.4% difference) within the same hour the flasks were taken indicating that it was acceptable to use the CO observations at 100m. A comparison of the concentration of CH_4 and CO_2 in the flask samples vs. the respective time matched *in situ* observations at 185m showed good agreement (less than 0.2% difference). The measurements are reported as dry air mole fractions in ppm (µmol mol^{-1}) and ppb (nmol mol^{-1}).

2.2 Sampling

The sampling procedure was based on the method used by the National Oceanic and Atmospheric Administration Carbon Cycle Greenhouse Gases (NOAA CCGG, (Lehman et al., 2013)). At MHD, the sampling of an additional flask for $^{14}CO_2$ analysis was added to the existing weekly NOAA CCGG flask sampling collection. A manual instantaneous sampling module was constructed for TAC, using a KNF Pump to pressurise and a Stirling cooler (Shinyei MA-SCUCO8) set to 0°C to dry the sample. Additionally, a 7-micron particle filter was added to avoid contamination of the sampling module and a check valve in addition to a toggle valve to ensure that existing measurements at the site were not influenced. A selection of tests, including a side-by-side comparison with the NOAA CCGG sampling unit at MHD, were performed before deployment to TAC. At TAC, samples were collected weekly into 2 L glass flasks (NORMAG, Germany, based on the NOAA CCGG design).

3 Methods

3.1 NAME simulations

Mole fractions were simulated at each measurement site using the Lagrangian particle dispersion model NAME (Numerical Atmospheric dispersion Modelling Environment) developed by the UK Met Office (Jones et al., 2007). Hypothetical particles are released into the model atmosphere at a rate of 10,000 per hour at the location of the observation site and transported backward in time for 30 days. It is assumed that when a particle resides in the lowest 0 - 40 m of the model atmosphere, pollution from ground-based emission sources is added to the air parcel (Arnold et al., 2018; Manning et al., 2011). The particle residence times in this surface layer are integrated over the 30-day simulation to calculate a "footprint" of each measurement that quantifies the sensitivity of the observation to a grid surrounding the measurement site (Manning et al., 2011). These footprints can be multiplied by flux fields to simulate the mole fraction due to each source at each instant in time. An example of such a footprint, also called back trajectory, can be found in the supplement (S2). In a similar fashion the NAME model can be run forward in time to simulate the concentration of a substance in the modelling domain. To simulate the concentration of a substance in the modelling domain, theoretical particles are released at the emission source location (point sources and area sources) with a rate that is relative to the emission source strength. We separate the CO_2 mole fraction into a background concentration $CO_{2\,bg}$ and a contribution from each source *i*:

$$CO_2 = CO_{2\,bg} + \sum{}_i CO_{2,i} \tag{1}$$

The background concentration can be determined by applying statistical methods to high-frequency observations (Barlow et al., 2015; Ruckstuhl et al., 2012) or estimated by models (Balzani Lööv et al., 2008; Lunt et al., 2016). In this work, high-frequency data existed only for $^{12}CO_2$ but not its isotopes and there was no model-derived background available for the isotopes, therefore, MHD data was used as background for the simulation of all CO_2 isotopes. While $^{13}CO_2$ and $^{14}CO_2$ measurements in MHD were selectively sampled during clean air conditions (high wind speeds from the Atlantic Ocean) the high frequency $^{12}CO_2$ data also contained pollution events. To exclude the pollution events, a rolling 15 percentile value (± 20 days) was calculated and used as $^{12}CO_2$ background. The 15th percentile of the MHD data was chosen for the background curve over other percentiles because it successfully removed short term concentration changes and pollution events. In addition to creating a smooth curve, the 15th percentile of the MHD data also fitted low concentrations observed in TAC, outside of the growing seasons (not much CO_2 uptake due to photosynthesis), well. Similarly, for the $^{13}CO_2$ and $^{14}CO_2$ background rolling median values (± 30 days) were calculated. These rolling median values created a smoother seasonal cycle compared to using the closest observed value.

3.2 Isotope Modelling

This section describes the method and the equations used to model $^{12}CO_2$, $^{13}CO_2$ and $^{14}CO_2$ at TAC. The modelling of the two stable CO_2 isotopes was necessary in order to be able to simulate the $^{14}CO_2$. A framework to simulate $^{14}CO_2$ was developed as a tool to investigate the observations and possible constraints of the radiocarbon method. A basic mass balance (Equation 1) was used as the basis of the modelling. Where the observed atmospheric mole fraction of $CO_{2\,obs}$ can be described as the sum of CO_2 from individual sectors ($CO_{2\,i}$) and a background contribution. This simple concept was adapted to the different CO_2 isotopes, by using the definition of the small delta (δ) value for $^{13}CO_2$ and the definition of the large delta (Δ) $^{14}CO_2$ as defined in Stuiver & Polach (1977). The simulated $^{13}CO_2$ was calculated with Equation 2 and the $\Delta^{14}CO_2$ with Equation 3. A detailed description on how Equation 2 and Equation 3 were derived can be found in the supplementary material S.3.

$$\delta^{13}CO_2 = \left(\frac{ \frac{ \sum\left(\left(\frac{\delta^{13}CO_{2\,i}}{1000} + 1 \right) \times {}^{12}CO_{2\,i} \times {}^{13}R_{std} \right) + {}^{13}CO_{2\,bg} }{ {}^{12}CO_2 } }{ {}^{13}R_{std} } - 1 \right) \times 1000 \tag{2}$$

Here, $\delta\,^{13}CO_{2\,i}$ is the $^{13}CO_2$ signature of emission source sector i [‰], $^{13}CO_{2\,bg}$ is the background $^{13}CO_2$ abundance from the rolling (± 30 days) median values of the MHD observations, $^{12}CO_{2\,i}$ = abundance of $^{12}CO_2$ from sector i [mol mol^{-1}] as simulated in TAC (Equation 1), $^{13}R_{std}$ is the ratio of reference standard [(mol mol^{-1})/ (mol mol^{-1})] and $^{12}CO_2$ is the total $^{12}CO_2$ enhancement [mol mol^{-1}] from Equation 1.

$$\Delta^{14}CO_2 = \left(\frac{\frac{\Sigma\left(\frac{\left(\frac{\Delta^{14}CO_{2\,i}}{1000}+1\right)\times {}^{14}R_{std}}{1-2\times\frac{25+\delta^{13}C_{\ i}}{1000}}\times {}^{12}CO_{2\,i}\right)}{{}^{12}CO_2}\times\left(1-2*\frac{25+\delta^{13}C_{\ 2}}{1000}\right)}{{}^{14}R_{std}} - 1 \right) \times 1000 \quad (3)$$

Where, $\Delta\,^{14}CO_{2\,i}$ is the $^{14}CO_2$ signature of emission source sector i [‰], $^{12}CO_{2\,i}$ is the abundance CO_2 from sector i [mol mol^{-1}]from Equation 1, $^{14}R_{std}$ is the ratio of reference standard [(mol mol^{-1})/ (mol mol^{-1})], $^{12}CO_2$ is the total CO_2 mole fraction [mol mol^{-1}] from Equation 1 and $\delta\,^{13}CO_2$ is the $^{13}CO_2$ signature [‰] from Equation 2.

The $\Delta^{14}C$ is normalized to a $\delta^{13}C$ value of -25 ‰, this is done to account for fractionation of the sample. Fractionation is the discrimination against one isotope in favour of the other in physical processes and chemical reactions. This discrimination takes place as the additional neutron in ^{13}C alters both the weight of the carbon and their chemical bonding energies. Biological processes such as for example photosynthesis selectively favour the lighter isotope. Fractionation effects discriminate against ^{14}C approximately twice as much as for ^{13}C (Fahrni et al., 2017; Stuiver and Polach, 1977). Normalising $\delta^{14}C$ measurements to a common $\delta^{13}C$ removes reservoir specific differences that are caused by fractionation.

For this work, sector-specific emissions reported in EDGAR v4.2 from year 2010 (Olivier et al., 2014) were used for the simulations of anthropogenic emissions and the National Aeronautics and Space Administration Carnegie Ames Stanford Approach (NASA CASA) emissions for biogenic emissions (Potter, 1999). It is assumed that all emissions reported in EDGAR correspond to $^{12}CO_2$ emissions. A detailed list of source sectors and associated isotopic signatures can be found in the supplementary data (S.4). All fossil sources were considered to have a $\Delta^{14}CO_2$ value of -1000 ‰.

3.3 Determination of fossil fuel CO_2 with $\Delta^{14}CO_2$ observations

The $\Delta^{14}CO_2$ observations at TAC and MHD were used to calculate the recently added CO_2 from fossil fuel burning ($ffCO_2$). This method takes advantage of the fact that fossil fuels have been isolated from other carbon pools for so long that they are completely devoid of ^{14}C, recent additions of CO_2 from fossil fuel burning therefore lead to a depletion in the atmospheric $\Delta^{14}CO_2$. We followed the approach of Turnbull et al., 2009, this approach was chosen as the calculation of the uncorrected $ffCO_2$ is separated from the corrections. This means that each correction can be evaluated for its impact on the final $ffCO_2$ value individually. The equation given in Turnbull et al., 2009 was adapted to have a correction term for heterotrophic respiration (section 3.3.1) and emissions from the nuclear industry (section 3.3.2) and is given in Equation 4. The reasoning behind the need for the corrections for heterotrophic respiration and emissions from the nuclear industry are explained in detail in the next two sections.

$$CO_{2\,ff} = \frac{CO_{2\,bg}\,(\Delta_{obs}-\Delta_{bg})}{(\Delta_{ff}-\Delta_{obs})} - \frac{CO_{2\,hr}\,(\Delta_{hr}-\Delta_{obs})}{(\Delta_{ff}-\Delta_{obs})} - \frac{CO_{2\,nuc}(\Delta_{nuc}-\Delta_{obs})}{(\Delta_{ff}-\Delta_{obs})} \quad (4)$$

Here $CO_{2\,ff}$ describes the recently added mole fraction from fossil fuel burning. $CO_{2\,bg}$ describes the background mole fraction. The rolling 15 percentile value (± 20 days) of the high frequency CO_2 observations at MHD (background site) was used as $CO_{2\,bg}$. For the Δ_{bg}, the rolling median value of the $\Delta^{14}CO_2$ flask measurements at MHD were calculated within a time window of ±20 days of the Δ_{obs}. Figure S.9 in a plot of the supplementary shows the MHD $\Delta^{14}CO_2$ observations and the rolling media value of the data used as Δ_{bg}. The use of the 15th percentile for the high frequency CO_2 data and the median for the $\Delta^{14}CO_2$ for weekly flask sampling (targeting background conditions) is consistent with the values used in the $\Delta^{14}CO_2$ modelling in section 3.1. $CO_{2\,obs}$ corresponds to the observed CO_2 mole fraction in the flask measurements at TAC (polluted site) while Δ_{obs} refers to the $\Delta^{14}CO_2$ measured from those same flasks. The Δ_{ff} describes the $^{14}CO_2$ signature of fossil fuel burning, this was assumed to be -1000‰. Equation 4 also contains two correction terms, one for nuclear emissions and one for heterotrophic respiration. In addition to these two correction terms explained below, other work (Graven et al., 2012; Turnbull et al., 2009b), investigated corrections for cosmogenic ^{14}C production and for the ocean atmosphere CO_2 exchange, for both corrections the modelled values are generally smaller than the uncertainty of the $\Delta^{14}CO_2$ measurements and they were therefore considered negligible for this work. $CO_{2\,hr}$ corresponds to the mole fraction of CO_2 at TAC that originates from heterotrophic respiration, while the Δ_{hr} is the $\Delta^{14}CO_2$ signature of heterotrophic respiration; both values were obtained by models as described in section 3.3.1. The Δ_{nuc} is the $\Delta^{14}CO_2$ signature of pure $^{14}CO_2$ emissions ($\Delta_{nuc} \approx 7.3\text{x}10^{14}$ ‰ (Bozhinova et al., 2014)) from nuclear sites and $CO_{2\,nuc}$ the mole fraction of CO_2 from nuclear emission at TAC (this value is obtained by modelling as described in 3.3.2). It is important to note that all approaches used determine $ffCO_2$ from $\Delta^{14}CO_2$ observations make certain assumptions, the method used here and described in detail in Turnbull et al., 2009, assumes that CO_2 emitted from autotropic respiration has the same $\Delta^{14}CO_2$ signature as the observations (Δ_{obs}), Section 3.3.1 goes in to more detailed why this is a reasonable assumption to make. All values used in the calculation of $CO_{2\,ff}$, including the Δ_{obs} and the Δ_{bg} and the correction terms have been included in the supplementary material in Table S10.

3.3.1 Biospheric correction

In the 1950s and 1960s extensive nuclear weapon tests caused a sudden sharp increase in the atmospheric $^{14}CO_2$ content, this is commonly referred to as the bomb spike (Levin et al., 1980; Manning et al., 1990). This bomb $^{14}CO_2$, has gradually been assimilated into other carbon pools (see S.5 in the supplement). Carbon that is exchanged from the biosphere to the atmosphere can have a different $\Delta^{14}CO_2$ signature depending on when the carbon was originally assimilated in to the biosphere. To account for this, biospheric emissions were split into two sources, autotrophic and heterotrophic. Autotrophic respiration of plants generally contains recently assimilated carbon (<1 year). Therefore, $^{14}CO_2$ from autotrophic respiration is generally assumed to be in equilibrium with the atmosphere. While recent work has indicated that autotrophic respiration may also contain older carbon (Phillips et al., 2015), it is assumed to be negligible for this work. Heterotrophically respired CO_2 contains carbon from older pools (for example decaying biomass) and can be significantly enriched in ^{14}C compared to current atmospheric CO_2 (Naegler and Levin, 2009). To simulate the $\Delta^{14}CO_2$ from heterotopic respiration, the 1-box model developed by (Graven et al., 2012) was used, it is assumed that two-thirds of heterotrophic respiration originates from older carbon pools. This resulted in a $\Delta^{14}CO_{2HR}$ of 67-91‰ for 2014-2015. For the calculation of $ffCO_2$ with Equation 4, 80‰ was used as the $^{14}CO_2$ signature of heterotrophic respiration (Δ_{HR}). The mole fraction enhancement due to CO_2 emitted from heterotrophic respiration ($CO_{2\,HR}$) was derived from the NASA CASA biosphere model and atmospheric back trajectories (more details about the modelling can be found in section 3.1). A similar disequilibrium exists with between the atmosphere and the ocean, but it was considered negligible for this work.

3.3.2 Nuclear correction

Radiocarbon emissions from nuclear reactors have a large temporal variability, making them difficult to correct for. Although the emissions are small, they have a $\Delta^{14}C$ value of ~7.3x10$^{\wedge 14}$ ‰, and can, therefore, influence radiocarbon observations significantly. During the study period, 3 types of nuclear power plants were in operation in the UK (Figure 1). Of these, both the AGR and the Magnox Reactor are cooled with CO_2 gas. This creates an oxidising condition in the reactor, resulting in the majority of the released ^{14}C being released in the form of $^{14}CO_2$. ^{14}C is produced in the reactor from reactions of neutrons with ^{14}N, ^{13}C, ^{17}O. Most of the $^{14}CO_2$ emitted from the AGRs and Magnox plants originates from N_2 impurities in the cooling gas (Yim and Caron, 2006). The UK also has one running pressurised water reactor (PWR), Sizewell B (52.21 °N, 1.62 °E), in the east of England. PWR contain a reducing reactor environment, leading to ^{14}C being released predominantly in the form of $^{14}CH_4$. As ^{14}C is constantly produced in nuclear reactors, parameterized emissions (an average emission factor per plant type that is multiplied with the power production of a plant) are a good approximation. However, the production of ^{14}C is highly dependent on the number of impurities present in the reactor and only a small part of the produced ^{14}C is ever emitted. Emissions can be caused by leakage as well as operational procedures, known as blowdown events. Reported emissions are therefore more informative. To apply a correction for these nuclear industry emissions in the calculation of $ffCO_2$ in Equation 4, 7.3x10^{14} ‰ was used as the Δ_{nuc}. To calculate the mole fraction of CO_2 derived from the nuclear industry ($CO_{2\,nuc}$ in Equation 4) atmospheric back trajectories where multiplied with a $^{14}CO_2$ emission map of reported nuclear industry emissions that was especially created for this study. This $^{14}CO_2$ emissions map was created with the highest frequency data available from each nuclear site. Monthly atmospheric emission data were provided by the two operators of the ten UK nuclear power plants; EDF and Magnox Ltd. Data for the other seventeen UK nuclear sites were taken from the annual Radioactivity in Food and the Environment RIFE, 1995-2016 (Enviroment Agency, Natural Resources Wales, 2017). The emissions from other European nuclear power plants were sourced from annual environmental reports if available (France, Germany) otherwise parameterized emissions were calculated according to (Graven and Gruber, 2011). The largest emitter of ^{14}C during the study period was the nuclear fuel reprocessing site in La Hague, Northern France (49.68 °N, 1.88 °W). For nuclear fuel reprocessing site in La Hague, monthly emission data reported on their website were utilised, a table transcribing these reported emissions is included in the supplementary material (S.6).

4 Results

4.1 Comparison of modelled and observed data

For this work $^{12}CO_2$, $\delta^{13}CO_2$ and $\Delta^{14}CO_2$ were simulated using Equation 1, 2 and 3 at TAC and are compared with observations in Figure 2. Daily mean values (24h) are displayed for both the modelled (blue line) and the observed data (black line, points). The uncertainty estimate (light blue area) includes the baseline uncertainty as well as the emission inventory uncertainty. The uncertainties were investigated by calculating a Monte Carlo ensemble of model runs (4000 runs) with perturbed background concentrations and sector-specific emissions. The background concentration was randomly altered within a factor of two of the measurement uncertainty. The sector-specific emission maps were multiplied with a randomly generated matrix, that let the emission in each grid cell vary between 50 – 150%. The shaded green areas represent the 95 % confidence interval uncertainty of these simulations. The TAC observations generally match the simulations well for $^{12}CO_2$ and $^{14}CO_2$. The exception is a large $^{12}CO_2$ peak in November 2014 that is significantly underestimated by the model. During the same time period, the two $^{14}CO_2$ samples taken were more depleted than the $^{14}CO_2$ simulations.

The $\delta^{13}CO_2$ simulations (Figure 2) show comparatively large uncertainties, this uncertainty is dominated by the variation of the net ecosystem exchange flux (from NASA CASA) during the Monte Carlo runs described above. The variation of the net ecosystem exchange flux has an ostensibly larger influence on the $^{13}CO_2$ simulations (compared to the $^{12}CO_2$ and $^{14}CO_2$) as carbon uptake and respiration cause strong fractionation in the atmosphere. This fractionation was captured in the model and the uncertainty estimation by assigning a $\delta^{13}CO_2$ signature to the net ecosystem exchange flux (see Equation 2 in Section 3.2 and table S.4 in the supplement). The close fit of the observations to the median of the simulations indicates that the variability of the $\delta^{13}CO_2$ signature of the net ecosystem exchange flux might have been overestimated.

For the $^{14}CO_2$ simulations as shown in Figure 2, the calculated uncertainty estimate was ± 5 ‰ or ~ 1.8 ppm in $ffCO_2$ equivalent. The term fossil fuel equivalent is used to describe how much recently emitted fossil fuel would have to be present in a sample to cause the equivalent depletion in ‰ in ^{14}C, the exact conversion from one to the other depends this was predominantly influenced by the uncertainty of the background value, as this was chosen to be double the measurement uncertainty (> ± 4 ‰). This is not surprising as the $\Delta^{14}CO_2$ observations have a large measurement uncertainty (1.8 ‰, ~ 0.72 ppm $ffCO_2$ equivalent) associated with them, and the measurement uncertainty was chosen as an indication of the background uncertainty. However, it emphasizes that strong $ffCO_2$ signals are needed in order to obtain $\Delta^{14}CO_2$ observations that can be distinguished from the background. At TAC, the fossil fuel influence is not always large enough to exceed this threshold.

4.2 Fossil Fuel CO_2 derived from $\Delta^{14}CO_2$ observations

This paper aims to determine if $\Delta^{14}CO_2$ observations can be used to estimate $ffCO_2$ at the TAC observation station in the UK. Multiple studies (Bozhinova et al., 2014; Graven and Gruber, 2011) have indicated that in some parts of the UK the radiocarbon method cannot be used as the large $^{14}CO_2$ emissions from nuclear sites would mask the depletion in the atmospheric $\Delta^{14}CO_2$

caused by recent fossil fuel emission. The flask sampling site in TAC was chosen deliberately following a preliminary study that suggested the influence from $^{14}CO_2$ from the nuclear industry at the TAC was moderate.

4.2.1 Influence of the corrections applied to the $ffCO_2$ calculation

During the calculation of the $ffCO_2$ with Equation 4, two correction terms were applied, one for heterotrophic respiration and one for the $^{14}CO_2$ emissions from the nuclear industry. The correction for heterotrophic respiration has to be applied at any site that could be influenced by biospheric fluxes (biospheric correction), while only sites located within the influence of nuclear industry sites have to apply the correction from nuclear industry emissions (nuclear correction). The biospheric and nuclear corrections were calculated using Equation 4 and as outlined in Sections 3.3.1 and 3.3.2. In Figure 3, the biospheric and nuclear corrections were calculated for the whole study period (2014-2015). To facilitate the comparison of their impact on the final $ffCO_2$ correction both the biospheric correction and the nuclear correction are displayed in $ffCO_2$ equivalent (unit of the individual correction terms in equation 4). The points in Figure 3 represent times when flask samples were taken at TAC. Since we aim to assess if TAC is a suitable site to derive $ffCO_2$ from $\Delta^{14}CO_2$ observations, the influence of the nuclear and biospheric corrections were assessed for the whole study period. The mean of the correction applied was 0.34 ppm $ffCO_2$ equivalent for the heterotrophic respiration and 0.25 ppm for the nuclear emissions. This means that the average nuclear correction over the whole study period at TAC for radiocarbon derived $ffCO_2$ is similar in magnitude to the correction for heterotrophic respiration. The maximum value calculated for the nuclear correction was 1.60 ppm $ffCO_2$ equivalent, similar to the highest biospheric correction value (1.23 ppm). For the nuclear correction, the fuel reprocessing site in La Hague and the nuclear power plant in Sizewell have the largest influence on the air parcels arriving at TAC. The fuel reprocessing site in La Hague because it is the highest ^{14}C emitter, and the nuclear power plant in Sizewell as it is spatially close, 50 km south east of TAC.

The average corrections applied for the heterotrophic respiration and the nuclear industry emissions are much smaller than the combined measurement uncertainty of the radiocarbon method to calculate $ffCO_2$ (± 5 ‰ ~ 1.8 ppm $ffCO_2$ equivalent). The observed $ffCO_2$ signal in TAC is frequently (50% of observations) smaller than the measurement uncertainty of the radiocarbon method. Note should be taken that the nuclear correction is based on reported monthly emission data from the operational UK nuclear power plants (Section 3.3.2). This temporal resolution does not capture complete reactor blowdowns before maintenance shut downs of nuclear power plants. The $^{14}CO_2$ emissions during these blowdown events can be 10 times higher than during standard operation. It is our opinion that these larger emissions before reactor maintenance are the cause of the very enriched data point of over 50 ‰ (Figure 3) on the 13th June 2014. The size of the nuclear correction calculated for the 13th June 2014 was 0.017 ppm, this obviously severely underestimates the nuclear enhancement observed in the sample. Back trajectories associated with this sample (S.2 in supplement) show that air masses originated from the North West of England where two nuclear power plants (Heysham 1&2 (54.03 °N, 2.92 °W)) and a nuclear fuel processing site (Sellafield (54.42 °N, 3.50 °W)) are situated. Heysham 1 was shut down for an in-depth boiler inspection (Office for Nuclear Regulation, 2014) on the 10th June 2014, emissions caused by this shut down could potentially explain the high $\Delta^{14}CO_2$ value observed on the 13th June 2014 at TAC.

4.2.2 Results of $ffCO_2$ derived from $\Delta^{14}CO_2$ observations at TAC

This section presents the results of the radiocarbon method that were gained from the $\Delta^{14}CO_2$ measurements performed at the TAC and MHD observation sites All the data presented in this section is available on the CEDA database (http://data.ceda.ac.uk/badc/gauge/data/tower/). In Figure 4 we present the $ffCO_2$ calculated with the radiocarbon method (Equation 4) from $\Delta^{14}CO_2$ observations at TAC station ($ffCO_{2\ observed}$) and compare it with simulated mixing ratios derived from modelling using emission inventories as described in Section 3.1 ($ffCO_{2\ simulated}$). 1 ppm of $ffCO_2$ causes a depletion of approximately 2.5 ‰ in $\Delta^{14}CO_2$. Figure 4 shows that most observed values are not significantly different from the modelled values. This implies that the $ffCO_2$ derived from $\Delta^{14}CO_2$ observations at TAC agrees well with the values simulated using emissions inventories (EDGAR 2010) and an atmospheric model (Section 3.2). However, the uncertainties associated with the observed $ffCO_2$ are relatively large, while the $ffCO_2$ mole fractions observed at TAC are comparatively low.

The very enriched $\Delta^{14}CO_2$ value observed on the 13th June 2014 was excluded from this analysis, this sample was likely influenced by $^{14}CO_2$ emissions from a nuclear reactor shut down as explained in Section 4.2.1. Figure 2 shows two other values that were excluded, both in November 2014. These observations were strongly depleted in $^{14}CO_2$ and coincided with a CO_2 enhancement that lasted approximately two weeks. Footprints calculated during this period indicate that the high CO_2 abundance observed is associated with an accumulation of emissions from a large geographical area over the UK and North-West Europe, due to an extended period of low wind speeds, during which the model appears to significantly underestimate the amplitude of the CO_2 peak. The two $\Delta^{14}CO_2$ measurements taken during this period were excluded from further analysis for two reasons: Firstly, because the $ffCO_2$ signal of those two points is so strong that it distorts the interpretation of all the other observations. Secondly because it is likely that the model would not represent the conditions during that period well (in extended period of low wind speeds the modelled wind speed and direction have considerable uncertainty and variability due to the dominant influence of local terrain features that are sub-grid scale and therefore not resolved).

4.2.3 Increasing the temporal resolution of ffCO2 using CO ratios

Carbon monoxide (CO) is a product of incomplete combustion and as such is co-emitted with the CO_2 produced by complete combustion. CO emissions can be expressed as a ratio relative to the fossil fuel CO_2 emissions. The emitted CO/ CO_2 ratio varies depending on the emission source. According to the NAEI 2014, UK gas power plants (1.0 ppb (CO) ppm $(CO_2)^{-1}$) and cars (0.5 ppb (CO) ppm $(CO_2)^{-1}$) under ideal driving conditions have low emission ratios, while larger vehicles preforming a cold start or accelerating on the motorway can have an emission factor an order of magnitude larger.$\Delta^{14}CO_2$-derived $ffCO_2$ is an expensive measurement often performed at low temporal resolution. Therefore, to maximise the scientific value of low frequency $ffCO_2$ observations, $ffCO_2$ has been used to calibrate the CO_{enh}/ $ffCO_2$ ratio for an individual sampling site (CO_{enh} = CO_{obs}-CO_{bg}) (Ammoura et al., 2016; Levin and Karstens, 2007; Miller et al., 2012; Turnbull et al., 2006; Vardag et al., 2015). The 15th percentile of the MHD CO data was used as the background (CO_{bg}). For CO_{obs}, time-matched TAC observations from the 100 m inlet line were used. To estimate the CO ratio at TAC during the study period, the CO_{enh} calculated as described above was plotted against the $ffCO_2$ derived from the radiocarbon method in Figure 5. The slope of the linear regression calculated for the CO_{enh}/ $ffCO_2$ plot shown in Figure 5 corresponds to the CO ratio. To estimate the uncertainty associated with the linear regression, the data was randomly resampled 10,000 times, while each value was allowed to vary within their measurement uncertainty. The measurement uncertainties were estimated at 1.8 ppm for $ffCO_2$ and 2 ppb for CO_{enh}. The CO ratio was calculated in this way for the whole dataset as well as different subsets, a list of the results can be found in Table 2. The median CO_{enh}/ $ffCO_2$ ratio over the whole sampling period was 5.7 (2.4-8.9) ppb ppm^{-1}, with a median R^2 correlation coefficient of 0.50. The CO_{enh} / $ffCO_2$ ratio usually has a better correlation in winter because the fossil fuel fluxes are larger (Miller et al., 2012; Vogel et al., 2010). Restricting the analysis to include only samples taken in winter results in a CO_{enh} / $ffCO_2$ ratio of 4.7 (1.0-10.1) ppb ppm^{-1}, with a median R^2 of 0.7 (0.1-1.0). It is assumed that the higher variability in the CO_{enh} / $ffCO_2$ ratio calculated from samples taken in winter only compared to the ratio obtained from all values is due to the lower amount of data points taken in winter rather than a genuinely higher variability of the CO_{enh} / $ffCO_2$ ratio at TAC in winter. The CO_{enh} / $ffCO_2$ ratio where all data points are used (5.7 ppb ppm^{-1}) is similar to the ratio obtained by the model (5.1 ppb ppm^{-1}) for the TAC site. Other studies have found a wide variety of CO_{enh} / $ffCO_2$ ratios, generally older studies have a higher CO_{enh} / $ffCO_2$ ratio such as Turnbull et al., 2006 with 20 ±5 ppb ppm^{-1} or Vogel et al., 2010 with 14.8 ppb ppm^{-1}, whereas more recent studies in Europe have found similar CO_{enh} / $ffCO_2$ such as Vardag et al., 2015 in Germany 5 ±3 ppb ppm^{-1} and Ammoura et al., 2016 in France 3.0-6.8 ppb ppm^{-1}. However, it is important to note that, in reality, the individual a CO_{enh} / $ffCO_2$ ratio varies for every measurement. This is because at each point in time, the station can be influenced by different combinations of emission source sectors, each with an emission ratio that may also vary significantly with time. The sector-specific simulations, included in the supplementary material (S.7), show that one of the dominant emission source sectors observable at TAC is road transport, an emission source with an inherently large variability in CO / CO_2 emission ratios. The CO / CO_2 emission ratio of road transport is dependent on fuel type, type of car and how it is driven (more emissions during cold starts and stop - start as opposed to a constant speed). While we expect to see an integrated emission signal from traffic at a tall tower site like TAC, each sample integrates air over a slightly different area with variable contributions from highways, country roads and city traffic. It is important to note that other source sectors have variable CO emission factors as well, for example in the sector domestic heat production, each individual boiler will have a different CO emission factor depending on the fuel source used and how optimised the operation conditions are. In addition to that $\Delta^{14}CO_2$ observations at TAC have predominantly been timed to take place in the afternoon, this might bias the calculated CO ratio to be more representative for daytime observations. If we take the average CO_{enh} / $ffCO_2$ ratio in TAC (5.7 ppb ppm^{-1}) as calculated above and multiply it with the high frequency CO_{enh} (as defined above), we get back a high frequency $ffCO_2$ time series for TAC. This time series of CO ratio derived $ffCO_2$

at TAC results in $ffCO_2$ values that are significantly larger than what the modelled $ffCO_2$ values suggest (simulated according to section 3.2, with the EDGAR 2010 fossil fuel emission map, Supplementary material S.8).

5 Discussion

This work evaluated the use of $\Delta^{14}CO_2$ observations to derive the amount of CO_2 from fossil fuel burning that was recently added to the atmosphere in the UK. It was suspected that the relatively high density of $^{14}CO_2$ emitting nuclear sites could mask any $\Delta\ ^{14}CO_2$ depletion caused by emissions from fossil fuel burning. It was found that while $^{14}CO_2$ emissions from nuclear industry sites in the UK do have an impact on $\Delta^{14}CO_2$ observations at a TAC; this influence is not prohibitive of utilising $\Delta^{14}CO_2$ observations for the determination of $ffCO_2$. However, the generally large uncertainties associated with $\Delta^{14}CO_2$ observations mean that at TAC, the observed depletion in $\Delta^{14}CO_2$ due to a $ffCO_2$ signal is often below the detection limit ($\Delta^{14}CO_2$ depletion <5‰ in about 50% of the flask samples). Other countries or locations without a large enough $ffCO_2$ signal to get a significant $\Delta^{14}CO_2$ depletion can use sampling techniques that integrate the $ffCO_2$ signal over weeks or months to increase the signal strength. In the UK, however, this would not be easily applicable as both the $^{12}CO_2$ from fossil fuel burning and the $^{14}CO_2$ from nuclear sites would be integrated. The correction for $^{14}CO_2$ emissions from nuclear industry sites would be difficult to apply, as long temporal integration of the sample would increase the chances of a routine blowdown or a maintenance event (with high $^{14}CO_2$ emissions) occurring at a nuclear reactor nearby.

Generally, the radiocarbon method of determining the $ffCO_2$ enhancement would perform better if stronger signals were encountered more frequently. To find sampling locations in the UK that would be suitable to use for determining $ffCO_2$ with the radiocarbon method a NAME forward model was used. A 1 year forward run was performed in NAME for both CO and $^{14}CO_2$ (June 2012-June 2013). CO was used as a proxy for fossil fuel CO_2 instead of the EDGAR 2010 emissions as there was a CO emission file correctly formatted for the use in NAME available to the authors. To convert the simulated CO values to $ffCO_2$ the CO_{enh} / $ffCO_2$ ratio of 5.7 ppb ppm^{-1}, determined in section 4.2.3, was used. These two simulations are then combined, dividing the average yearly increase in the $\Delta^{14}CO_2$ due to nuclear emissions ($\Delta^{14}CO_{2\ nuclear}$) by the average yearly decrease in the $\Delta^{14}CO_2$ signal due to emissions from fossil fuel burning ($\Delta CO_{2\ ff}$). This ratio, illustrated in Figure 6, indicates areas of the UK that would provide suitable sampling locations. A ratio lower than 1 indicates that on average the depletion due to fossil fuel burning is lower than the enhancement due to nuclear emissions and as such is a better location for radiocarbon measurements. A ratio of 1 indicates that on average, the depletion expected due to fossil fuel burning at a location, is equal to the enhancement due to emission from $^{14}CO_2$ from nuclear sites. It is important to recognise that this ratio is obtained by dividing simulated yearly averages, it therefore shows the locations that are on average favourable for $\Delta^{14}CO_2$ sampling. Locations that have a high ratio, are less likely to be suitable for $\Delta^{14}CO_2$ sampling, either because they are heavily influenced by $^{14}CO_2$ emissions from nuclear industry sites or because the site is unlikely to be exposed to large fossil fuel emissions. This work also aimed to evaluate if $ffCO_2$ derived from $\Delta^{14}CO_2$ observations could be used in inverse models to preform top down emission estimates. This work shows that although $ffCO_2$ derived with the radiocarbon method can be used to investigate national emissions, the relatively low depletion in $\Delta^{14}CO_2$ (due to $CO_{2\ ff}$) in well-mixed air masses over the UK mean that applying the method to city scale emissions, where emissions are closer and therefore less diluted, might be more suitable. Figure 6 shows that sampling stations located closer to a region with higher emissions such as Greater London are more likely to encounter $ffCO_2$ enhancements that would lead to significant and therefore measurable depletions in $\Delta^{14}CO_2$, this would optimise the scientific value of the cost-intensive $\Delta^{14}CO_2$ measurements. In addition, improving the precision of the correction terms applied to the $ffCO_2$ calculations is also important. This could be achieved through the provision of higher frequency nuclear industry emission data for $^{14}CO_2$ in the UK, improvements in the biospheric correction, and a reduction in the measurement uncertainties associated with $\Delta^{14}CO_2$ observations would also improve the usability of the radiocarbon method in the UK.

6 Conclusions

This study has provided valuable insights into the viability of using $\Delta^{14}CO_2$ measurements in the UK to determine recently emitted CO_2 from fossil fuel. It was shown that the UK fossil fuel emissions estimates from EDGAR are consistent with the observations. Despite the comparatively high density of $^{14}CO_2$ emitting nuclear reactors, corrections applied for nuclear emissions are not generally larger than those applied to account for the biospheric disequilibrium. However, both corrections add to the uncertainty of observed $ffCO_2$ values. The largest issue with using $^{14}CO_2$ observations at TAC for national emission estimates is that the measurement uncertainty is often higher than the observed and predicted depletion in radiocarbon. The derived $ffCO_2$: CO ratio is consistent with the inventory (NAEI 2014). Although, uncertainties are large and use of a simple ratio may not be accounted for all of the variability. The use of radiocarbon to estimate UK emissions could be improved in various ways. Higher frequency and automated samples allowing sampling at optimal time periods would be one way to address this, another would be selecting optimal sampling locations as illustrated in Figure 6. Prior to $^{14}CO_2$ analysis, assessment of the back trajectories and analysis of mole fraction trace compounds could be performed to ensure samples are collected during ideal conditions.

7 Author Contribution

Angelina Wenger developed the sampling equipment, maintained the measurements and carried out the research. Simon O'Doherty and Angelina Wenger designed the research. Katherine Pugsley and Angelina Wenger ran the isotope simulations. Simon O'Doherty provided CO_2 and CO data. Alistair Manning, Matt Rigby, Mark Lunt and Emily White ran NAME simulations and helped to analyse the model output. Katherine Pugsley and Angelina Wenger prepared the manuscript with contributions from all co-authors.

8 Acknowledgements

The authors would like to acknowledge Scott Lehman, Chad Wolak, Stephen Morgan and Patrick Cappa of the INSTAAR Laboratory for Radiocarbon Preparation and Research for the ^{14}C sample processing and Don Neff and the NOAA GMD team for the routing of the samples as well as the greenhouse gas analysis. Collection of radiocarbon measurements was funded by the NERC GAUGE programme under a grant to the University of Bristol NE/K002236/1.

References

Adams, M., Rypdal, K. and Woodfield, M.: EMEP/EEA air pollutant emission inventory guidebook 2016., 2016.

Ammoura, L., Xueref-Remy, I., Vogel, F., Gros, V., Baudic, A., Bonsang, B., Delmotte, M., Té, Y. and Chevallier, F.: Exploiting stagnant conditions to derive robust emission ratio estimates for CO2, CO and volatile organic compounds in Paris, Atmos. Chem. Phys., 16(24), 15653–15664, doi:10.5194/acp-16-15653-2016, 2016.

Arnold, T. ., Manning, A. . J. ., Kim, J. ., Li, S. ., Webster, H. ., Thomson, D. . and O'Doherty, S.: Inverse modelling of CF 4 and NF 3 emissions in East Asia, , 18, 13305–13320, doi:10.5194/acp-18-13305-2018., 2018.

Ballantyne, A. P., Andres, R., Houghton, R., Stocker, B. D., Wanninkhof, R., Anderegg, W., Cooper, L. A., DeGrandpre, M., Tans, P. P., Miller, J. B., Alden, C. and White, J. W. C.: Audit of the global carbon budget: Estimate errors and their impact on uptake uncertainty, Biogeosciences, 12(8), 2565–2584, doi:10.5194/bg-12-2565-2015, 2015.

Balzani Lööv, J. M., Henne, S., Legreid, G., Staehelin, J., Reimann, S., Prévôt, A. S. H., Steinbacher, M. and Vollmer, M. K.: Estimation of background concentrations of trace gases at the Swiss Alpine site Jungfraujoch (3580 m asl), J. Geophys. Res. Atmos., 113(22), 1–17, doi:10.1029/2007JD009751, 2008.

Barlow, J. M., Palmer, P. I., Bruhwiler, L. M. and Tans, P.: Analysis of CO2 mole fraction data: First evidence of large-scale changes in CO2 uptake at high northern latitudes, Atmos. Chem. Phys., 15(23), 13739–13758, doi:10.5194/acp-15-13739-2015, 2015.

BEIS, U.: Final UK Greenhouse gas emissions national statistic:1990-2016 (2016 UK ghg:final figures-statistical release), Dep. Business, Energy Ind. Strateg., (February) [online] Available from: https://www.gov.uk/government/statistics/final-uk-greenhouse-gas-emissions-national-statistics-1990-2016, 2018.

Berhanu, T. A., Szidat, S., Brunner, D., Satar, E., Schanda, R., Nyfeler, P., Battaglia, M., Steinbacher, M., Hammer, S. and Leuenberger, M.: Estimation of the fossil fuel component in atmospheric CO2 based on radiocarbon measurements at the Beromünster tall tower, Switzerland, Atmos. Chem. Phys., 17(17), 10753–10766, doi:10.5194/acp-17-10753-2017, 2017.

Bozhinova, D., Van Der Molen, M. K., Van Der Velde, I. R., Krol, M. C., Van Der Laan, S., Meijer, H. A. J. and Peters, W.: Simulating the integrated summertime δ14CO2 signature from anthropogenic emissions over Western Europe, Atmos. Chem. Phys., 14(14), 7273–7290, doi:10.5194/acp-14-7273-2014, 2014.

Bozhinova, D., Palstra, S. W. L., van der Molen, M. K., Krol, M. C., Meijer, H. A. J. and Peters, W.: Three Years of Δ14CO2 Observations from Maize Leaves in the Netherlands and Western Europe, Radiocarbon, 58(03), 459–478, doi:10.1017/RDC.2016.20, 2016.

Ciais, P., Paris, J. D., Marland, G., Peylin, P., Piao, S. L., Levin, I., Pregger, T., Scholz, Y., Friedrich, R., Rivier, L., Houwelling, S. and Schulze, E. D.: The European carbon balance. Part 1: Fossil fuel emissions, Glob. Chang. Biol., 16(5), 1395–1408, doi:10.1111/j.1365-2486.2009.02098.x, 2010.

Currie, L. A.: The remarkable metrological history of radiocarbon dating [II], J. Res. Natl. Inst. Stand. Technol., 109(2), 185, doi:10.6028/jres.109.013, 2004.

Enviroment Agency, Natural Resources Wales, F. S. A.: RIFE reports, [online] Available from: https://www.gov.uk/government/publications/radioactivity-in-food-and-the-environment-rife-reports-2004-to-2016, 2017.

Fahrni, S. M., Southon, J. R., Santos, G. M., Palstra, S. W. L., Meijer, H. A. J. and Xu, X.: ScienceDirect Reassessment of the 13 C / 12 C and 14 C / 12 C isotopic fractionation ratio and its impact on high-precision radiocarbon dating, Geochim. Cosmochim. Acta, 213, 330–345, doi:10.1016/j.gca.2017.05.038, 2017.

Friedlingstein, P., Houghton, R. A., Marland, G., Hackler, J., Boden, T. A., Conway, T. J., Canadell, J. G., Raupach, M. R., Ciais, P. and Le Quéré, C.: Update on CO2 emissions, Nat. Geosci., 3(12), 811–812, doi:10.1038/ngeo1022, 2010.

Gamnitzer, U., Karstens, U., Kromer, B., Neubert, R. E. M., Meijer, H. A. J., Schroeder, H. and Levin, I.: Carbon monoxide: A quantitative tracer for fossil fuel CO<inf>2</inf>?, J. Geophys. Res. Atmos., 111(22), 1–19, doi:10.1029/2005JD006966, 2006.

Graven, H. D. and Gruber, N.: Continental-scale enrichment of atmospheric 14CO 2 from the nuclear power industry: Potential impact on the estimation of fossil fuel-derived CO 2, Atmos. Chem. Phys., 11(23), 12339–12349, doi:10.5194/acp-11-12339-2011, 2011a.

Graven, H. D. and Gruber, N.: Continental-scale enrichment of atmospheric14CO2from the nuclear power industry: Potential impact on the estimation of fossil fuel-derived CO2, Atmos. Chem. Phys., 11(23), 12339–12349, doi:10.5194/acp-11-12339-2011, 2011b.

Graven, H. D., Guilderson, T. P. and Keeling, R. F.: Observations of radiocarbon in CO<inf>2</inf> at la Jolla, California, USA 1992-2007: Analysis of the long-term trend, J. Geophys. Res. Atmos., 117(2), 1–14, doi:10.1029/2011JD016533, 2012.

Gurney, K. R., Liang, J., Patarasuk, R., O'Keeffe, D., Huang, J., Hutchins, M., Lauvaux, T., Turnbull, J. C. and Shepson, P. B.: Reconciling the differences between a bottom-up and inverse-estimated FFCO2 emissions estimate in a large US urban area, Elem Sci Anth, 5(0), 44, doi:10.1525/elementa.137, 2017.

IPCC: Summary for Policymakers, IPCC, Genova, Switzerland., 2014.

Jones, A., Thomson, D., Hort, M. and Devenish, B.: The U . K . Met Office ' s next generation atmospheric dispersion model, NAME III, in UK Met Office, pp. 580–589, Met Office., 2007.

Lehman, S. J., Miller, J. B., Wolak, C., Southon, J. R., Trans, P. P., Montzka, S. a., Sweeney, C., Andrews, A., LaFranchi, B., Guilderson, T. P. and Turnbull, J. C.: Allocation of terrestrial carbon sources using \ce{^{14}CO2}: Methods, measurement, and modeling, Radiocarbon, 55(2–3), 1484–1495, doi:10.2458/azu_js_rc.55.16392, 2013.

Levin, I. and Karstens, U.: Inferring high-resolution fossil fuel CO2 records at continental sites from combined 14CO2 and CO observations, Tellus, Ser. B Chem. Phys. Meteorol., 59(2), 245–250, doi:10.1111/j.1600-0889.2006.00244.x, 2007.

Levin, I. and Kromer, B.: Twenty Years of Atmospheric 14CO2 Observations at Schauinsland Station, Germany, Radiocarbon, 39(2), 205–218, doi:10.2458/azu_js_rc.39.1942, 1997.

Levin, I., Munnich, K. and Weiss, W.: the Effect of Anthropogenic Co2 and C-14 Sources on the Distribution of C-14 in the Atmosphere, Radiocarbon, 22(2), 379–391, doi:10.2458/azu_js_rc.22.627, 1980.

Levin, I., Kromer, B., Schmidt, M. and Sartorius, H.: A novel approach for independent budgeting of fossil fuel CO_2 over Europe by $^{14}CO_2$ observations, Geophys. Res. Lett., 30(23), n/a-n/a, doi:10.1029/2003GL018477, 2003.

Lopez, M., Schmidt, M., Delmotte, M., Colomb, A., Gros, V., Janssen, C., Lehman, S. J., Mondelain, D., Perrussel, O., Ramonet, M., Xueref-Remy, I. and Bousquet, P.: CO, NOxand13CO2as tracers for fossil fuel CO2: Results from a pilot study in Paris during winter 2010, Atmos. Chem. Phys., 13(15), 7343–7358, doi:10.5194/acp-13-7343-2013, 2013.

Lunt, M. F., Rigby, M., Ganesan, A. L. and Manning, A. J.: Estimation of trace gas fluxes with objectively determined basis functions using reversible-jump Markov chain Monte Carlo, Geosci. Model Dev., 9(9), 3213–3229, doi:10.5194/gmd-9-3213-2016, 2016.

Manning, A. J., O'Doherty, S., Jones, A. R., Simmonds, P. G. and Derwent, R. G.: Estimating UK methane and nitrous oxide emissions from 1990 to 2007 using an inversion modeling approach, J. Geophys. Res. Atmos., 116(2), 1–19, doi:10.1029/2010JD014763, 2011.

Manning, M. R., Lowe, D. C., Melhuish, W. H., Sparks, R. J., Wallace, G., Brenninkmeijer, C. A. M. and McGill, R. G.: THE USE OF RADIOCARBON MEASUREMENTS IN ATMOSPHERIC STUDIES, Radiocarbon, 32(1), 37–58, 1990.

Miller, J. B., Lehman, S. J., Montzka, S. A., Sweeney, C., Miller, B. R., Karion, A., Wolak, C., Dlugokencky, E. J., Southon, J., Turnbull, J. C. and Tans, P. P.: Linking emissions of fossil fuel CO_2 and other anthropogenic trace gases using atmospheric $^{14}CO_2$, J. Geophys. Res. Atmos., 117(D8), n/a-n/a, doi:10.1029/2011JD017048, 2012.

Naegler, T. and Levin, I.: Observation-based global biospheric excess radiocarbon inventory 1963-2005, J. Geophys. Res. Atmos., 114(17), 1–8, doi:10.1029/2008JD011100, 2009.

Nisbet, E. and Weiss, R.: Top-Down Versus Bottom-Up, Science (80-.)., 328(June), 1241–1244, 2010.

Office for Nuclear Regulation: Office for Nuclear Regulation (ONR) Quarterly Site Report for Heysham Power Stations, 2014.

Olivier, J. G. ., Janssens-Maenhout, G., Muntean, M. and Peters, J. A. H. .: Trends in global CO2 emissions: 2014 Report., 2014.

Palmer, P. I., O'Doherty, S., Allen, G., Bower, K., Bösch, H., Chipperfield, M. P., Connors, S., Dhomse, S., Feng, L., Finch, D. P., Gallagher, M. W., Gloor, E., Gonzi, S., Harris, N. R. P., Helfter, C., Humpage, N., Kerridge, B., Knappett, D., Jones, R. L., Le Breton, M., Lunt, M. F., Manning, A. J., Matthiesen, S., Muller, J. B. A., Mullinger, N., Nemiitz, E., O'Shea, S., Parker, R. J., Percival, C. J., Pitt, J., Riddick, S. N., Rigby, M., Sembhi, H., Siddans, R., Skelton, R. L., Smith, P., Sonderfeld, H., Stanley, K., Stavert, A. R., Wenger, A., White, E., Wilson, C. and Young, D.: A measurement-based verification framework for UK greenhouse gas emissions: an overview of the Greenhouse gAs Uk and Global Emissions (GAUGE) project, Atmos. Chem. Phys. Discuss., 18(February), 1–52, doi:10.5194/acp-2018-135, 2018.

Phillips, C. L., Mcfarlane, K. J., Lafranchi, B., Desai, A. R., Miller, J. B. and Lehman, S. J.: Observations of 14CO2 in ecosystem respiration from a temperate deciduous forest in Northern Wisconsin, J. Geophys. Res. Biogeosciences, 120(4), 1–17, doi:10.1002/2014JG002808.Received, 2015.

Potter, C. S.: Terrestrial biomass and the effects of deforestration on the global carbon cycle, Bioscience, 49(10), 769–778, 1999.

Le Quéré, C., Andrew, R. M., Canadell, J. G., Sitch, S., Ivar Korsbakken, J., Peters, G. P., Manning, A. C., Boden, T. A., Tans, P. P., Houghton, R. A., Keeling, R. F., Alin, S., Andrews, O. D., Anthoni, P., Barbero, L., Bopp, L., Chevallier, F., Chini, L. P., Ciais, P., Currie, K., Delire, C., Doney, S. C., Friedlingstein, P., Gkritzalis, T., Harris, I., Hauck, J., Haverd, V., Hoppema, M., Klein Goldewijk, K., Jain, A. K., Kato, E., Körtzinger, A., Landschützer, P., Lefèvre, N., Lenton, A., Lienert, S., Lombardozzi, D., Melton, J. R., Metzl, N., Millero, F., Monteiro, P. M. S., Munro, D. R., Nabel, J. E. M. S., Nakaoka, S. I., O'Brien, K., Olsen, A., Omar, A. M., Ono, T., Pierrot, D., Poulter, B., Rödenbeck, C., Salisbury, J., Schuster, U., Schwinger, J., Séférian, R., Skjelvan, I., Stocker, B. D., Sutton, A. J., Takahashi, T., Tian, H., Tilbrook, B., Van Der Laan-Luijkx, I. T., Van Der Werf, G. R., Viovy, N., Walker, A. P., Wiltshire, A. J. and Zaehle, S.: Global Carbon Budget 2016, Earth Syst. Sci. Data, 8(2), 605–649, doi:10.5194/essd-8-605-2016, 2016.

Le Quéré, C., Andrew, R. M., Friedlingstein, P., Sitch, S., Pongratz, J., Manning, A. C., Ivar Korsbakken, J., Peters, G. P., Canadell, J. G., Jackson, R. B., Boden, T. A., Tans, P. P., Andrews, O. D., Arora, V. K., Bakker, D. C. E., Barbero, L., Becker, M., Betts, R. A., Bopp, L., Chevallier, F., Chini, L. P., Ciais, P., Cosca, C. E., Cross, J., Currie, K., Gasser, T., Harris, I., Hauck, J., Haverd, V., Houghton, R. A., Hunt, C. W., Hurtt, G., Ilyina, T., Jain, A. K., Kato, E., Kautz, M., Keeling, R. F., Klein Goldewijk, K., Körtzinger, A., Landschützer, P., Lefèvre, N., Lenton, A., Lienert, S., Lima, I., Lombardozzi, D., Metzl, N., Millero, F., Monteiro, P. M. S., Munro, D. R., Nabel, J. E. M. S., Nakaoka, S. I., Nojiri, Y., Antonio Padin, X., Peregon, A., Pfeil, B., Pierrot, D., Poulter, B., Rehder, G., Reimer, J., Rödenbeck, C., Schwinger, J., Séférian, R., Skjelvan, I., Stocker, B. D., Tian, H., Tilbrook, B., Tubiello, F. N., Laan-Luijkx, I. T. V., Werf, G. R. V., Van Heuven, S., Viovy, N., Vuichard, N., Walker, A. P., Watson, A. J., Wiltshire, A. J., Zaehle, S. and Zhu, D.: Global Carbon Budget 2017, Earth Syst. Sci. Data, 10(1), 405–448, doi:10.5194/essd-10-405-2018, 2018.

Roberts, M. and Southon, J.: A preliminary determination of the absolute 14C/12C ratio of OX-I, Radiocarbon, 49(2), 441–445 [online] Available from: http://darchive.mblwhoilibrary.org/handle/1912/4393, 2007.

Ruckstuhl, A. F., Henne, S., Reimann, S., Steinbacher, M., Vollmer, M. K., O'Doherty, S., Buchmann, B. and Hueglin, C.: Robust extraction of baseline signal of atmospheric trace species using local regression, Atmos. Meas. Tech., 5(11), 2613–2624, doi:10.5194/amt-5-2613-2012, 2012.

Stanley, K. M., Grant, A., O'Doherty, S., Young, Di., Manning, A. J., Stavert, A. R., Gerard Spain, T., Salameh, P. K., Harth, C. M., Simmonds, P. G., Sturges, W. T., Oram, D. E. and Derwent, R. G.: Greenhouse gas measurements from a UK network of tall towers: Technical description and first results, Atmos. Meas. Tech., 11(3), 1437–1458, doi:10.5194/amt-11-1437-2018, 2018.

Stuiver, M. and Polach, H.: Reporting of 14C Data, Radiocarbon, 19(3), 355–363, 1977.

Suess, H.: Radiocarbon Concentration in Modern Wood, Science (80-.)., 122(3166), 415–417, doi:10.1126/science.122.3166.415-a, 1955.

Turnbull, J., Rayner, P., Miller, J., Naegler, T., Ciais, P. and Cozic, A.: On the use of $^{14}CO_2$ as a tracer for fossil fuel CO_2: Quantifying uncertainties using an atmospheric transport model, J. Geophys. Res., 114(D22), D22302, doi:10.1029/2009JD012308, 2009a.

Turnbull, J., Guenther, D., Karion, A., Sweeney, C., Anderson, E., Andrews, A., Kofler, J., Miles, N., Newberger, T., Richardson, S. and Tans, P.: An integrated flask sample collection system for greenhouse gas measurements, Atmos. Meas. Tech., 5(9), 2321–2327, doi:10.5194/amt-5-2321-2012, 2012.

Turnbull, J. C., Miller, J. B., Lehman, S. J., Tans, P. P., Sparks, R. J. and Southon, J.: Comparison of 14CO2, CO, and SF6 as

tracers for recently added fossil fuel CO2 in the atmosphere and implications for biological CO2 exchange, Geophys. Res. Lett., 33(1), 2–6, doi:10.1029/2005GL024213, 2006.
Turnbull, J. C., Miller, J. B., Lehman, S. J., Hurst, D., Peters, W., Tans, P. P., Southon, J., Montzka, S. A., Elkins, J. W., Mondeel, D. J., Romashkin, P. A., Elansky, N. and Skorokhod, A.: Spatial distribution of 14 CO 2 across Eurasia: measurements from the TROICA-8 expedition, Atmos. Chem. Phys, 9, 175–187, doi:10.5194/acp-9-175-2009, 2009b.
Turnbull, J. C., Karion, A., Fischer, M. L., Faloona, I., Guilderson, T., Lehman, S. J., Miller, B. R., Miller, J. B., Montzka, S., Sherwood, T., Saripalli, S., Sweeney, C. and Tans, P. P.: Assessment of fossil fuel carbon dioxide and other anthropogenic trace gas emissions from airborne measurements over Sacramento, California in spring 2009, Atmos. Chem. Phys., 11(2), 705–721, doi:10.5194/acp-11-705-2011, 2011.
Turnbull, J. C., Sweeney, C., Karion, A., Newberger, T., Lehman, S. J., Cambaliza, M. O., Shepson, P. B., Gurney, K., Patarasuk, R. and Razlivanov, I.: Journal of Geophysical Research : Atmospheres, J. Geophys. Res. Atmos., 292–312, doi:10.1002/2014JD022555.Received, 2015.
Vardag, S. N., Gerbig, C., Janssens-Maenhout, G. and Levin, I.: Estimation of continuous anthropogenic CO2: Model-based evaluation of CO2, CO, δ13C(CO2) and Δ14C(CO2) tracer methods, Atmos. Chem. Phys., 15(22), 12705–12729, doi:10.5194/acp-15-12705-2015, 2015.
Vogel, F., Hammer, S., Steinhof, A., Kromer, B. and Levin, I.: Implication of weekly and diurnal 14 C calibration on hourly estimates of CO-based fossil fuel CO 2 at a moderately polluted site in southwestern Germany, Tellus, Ser. B Chem. Phys. Meteorol., 62B, 512–520, doi:10.1111/j.1600-0889.2010.00477.x, 2010.
Vogel, F., Levin, I. and Worthy, D. E. J.: Implications for Deriving Regional Fossil Fuel CO2 Estimates from Atmospheric Observations in a Hot Spot of Nuclear Power Plant 14CO2 Emissions, Radiocarbon, 55(3–4), 1556–1572, doi:10.2458/azu_js_rc.55.16347, 2013.
van Vuuren, D. P., Hoogwijk, M., Barker, T., Riahi, K., Boeters, S., Chateau, J., Scrieciu, S., van Vliet, J., Masui, T., Blok, K., Blomen, E. and Kram, T.: Comparison of top-down and bottom-up estimates of sectoral and regional greenhouse gas emission reduction potentials, Energy Policy, 37(12), 5125–5139, doi:10.1016/j.enpol.2009.07.024, 2009.
Xueref-Remy, I., Dieudonné, E., Vuillemin, C., Lopez, M., Lac, C., Schmidt, M., Delmotte, M., Chevallier, F., Ravetta, F., Perrussel, O., Ciais, P., Bréon, F. M., Broquet, G., Ramonet, M., Gerard Spain, T. and Ampe, C.: Diurnal, synoptic and seasonal variability of atmospheric CO2 in the Paris megacity area, Atmos. Chem. Phys., 18(5), 3335–3362, doi:10.5194/acp-18-3335-2018, 2018.
Yim, M. S. and Caron, F.: Life cycle and management of carbon-14 from nuclear power generation, Prog. Nucl. Energy, 48(1), 2–36, doi:10.1016/j.pnucene.2005.04.002, 2006.
Zhao, Y., Nielsen, C. P. and McElroy, M. B.: China's CO2emissions estimated from the bottom up: Recent trends, spatial distributions, and quantification of uncertainties, Atmos. Environ., 59, 214–223, doi:10.1016/j.atmosenv.2012.05.027, 2012.

Species, Site **Instrument**	**Scale** **Operator**
CO_2, TAC Picarro CRDS G2301, *in situ*	WMO x2007 University of Bristol
CO, TAC GCMD, *in situ*	CSIRO-98 University of Bristol

CO_2, MHD Picarro CRDS G2401, *in situ*	WMO x2007 LSCE
CO, MHD RGA, *in situ*	CSIRO-98 University of Bristol
CO_2, MHD + TAC NDIR, flask	WMO x2007 NOAA
CO, MHD + TAC Aerolaser VUV fluorimetry flask	WMO x2014 NOAA
$^{13}CO_2$, MHD + TAC IRMS, flask	PDB NOAA, INSTAAR
$^{14}CO_2$, MHD + TAC AMS, flask	NBS Oxalic Acid I NOAA, INSTAAR, UC Irvine

Table 1: Overview of greenhouse gas measurements presented in this paper. The acronyms used to describe instruments are Cavity Ring-Down Spectroscopy (CRDS), Gas Chromatography Mass Detector (GCMD), Residual Gas Analyser (RGA), Nondispersive Infrared Detector (NDIR), Vacuum Ultra Violet (VUV), Infrared Mass Spectrometry (IRMS), Accelerator Mass Spectrometry (AMS).

Data	R^2	ppm / ppb	P value
All	0.9 (0.5-0.9)	6.5 (4.8-7.9)	0.01
All (not Nov)	0.5 (0.2-0.7)	5.7 (2.4-8.9)	0.04
Winter only	1.0 (0.7-1.0)	6.6 (4.6-8.0)	0.03
Winter only (not Nov)	0.7 (0.1-1.0)	4.7 (1.0-10.1)	0.15

Table 2. CO ratios using a MHD 15th-percentile as background value under different times using NAEI 2012 emissions inventory and measurements at TAC. Uncertainties shown are the 5th and 95th percentile.

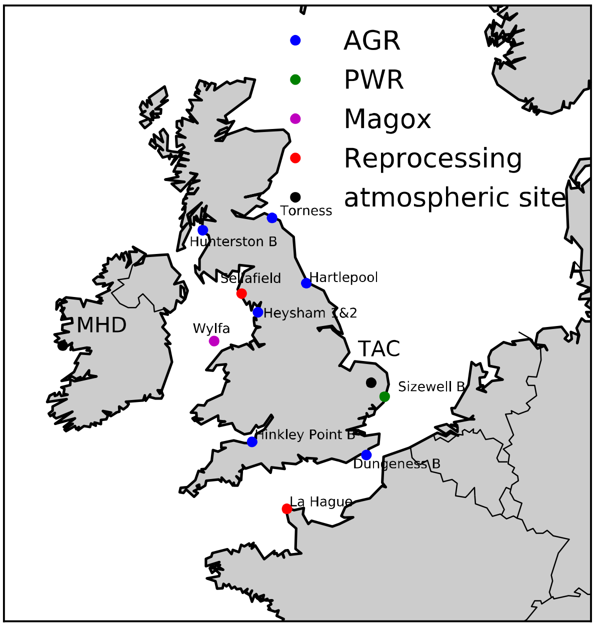

Figure 1. Map of Northern Europe nuclear power stations and other nuclear facilities. Reactor types are: Advanced Gas Reactor (AGR) (blue) and Pressurised Water Reactor (PWR) (green), Magnox (pink). Fuel reprocessing are labelled separately (red). The atmospheric measurement sites (TAC and MHD) are also labelled (black).

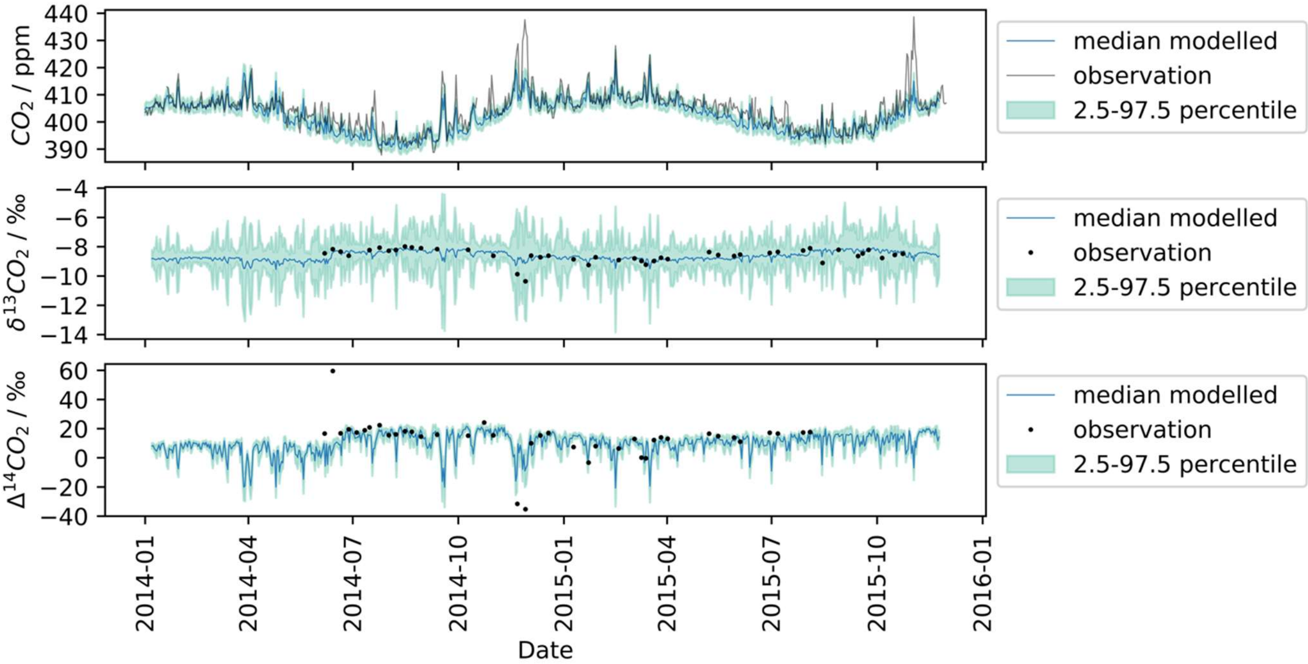

Figure 2. Comparison of modelled and observed CO_2 for each isotope at TAC. The black line and dots represent observations measured at the TAC field station. The blue line corresponds to the median modelled value (according to section 3.2). The shaded green area represents the uncertainty estimate for the modelled values based on the bootstrapping method described in section 4.1. The upper panel compares observed and modelled $^{12}CO_2$ values. The middle panel contains both modelled $^{13}CO_2$ and flask sampling based observations, while the lower panel shows the modelled and observed $^{14}CO_2$ data.

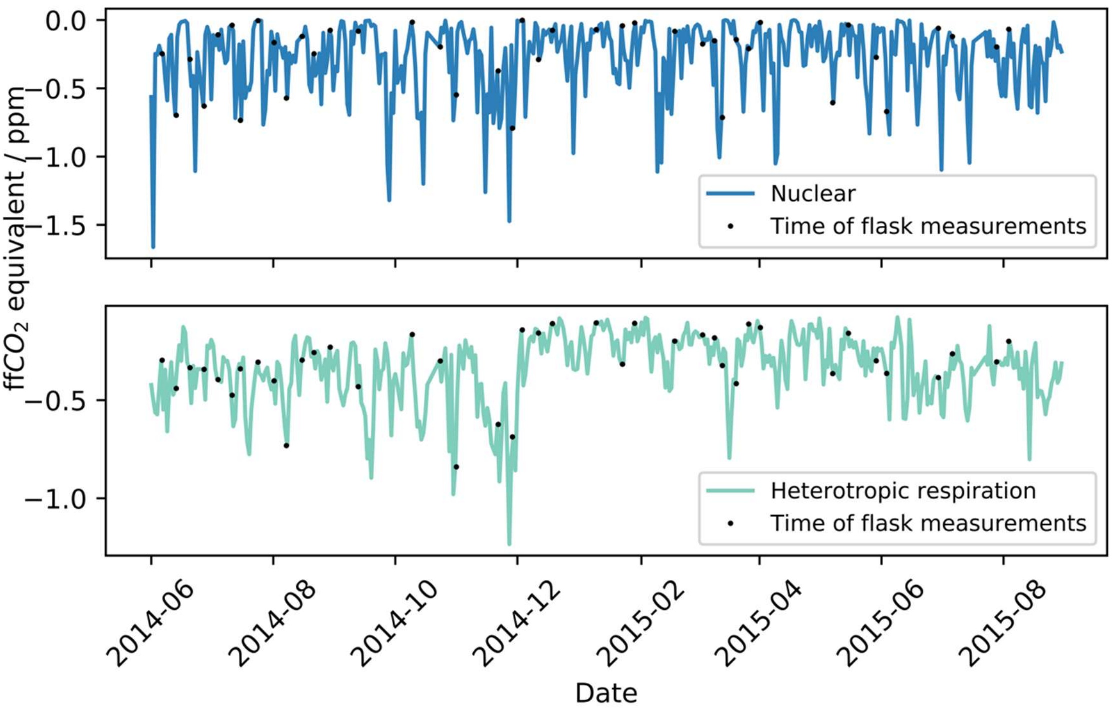

Figure 3. The blue line (upper panel) represents the ffCO_2 equivalent theoretical corrections that need to be applied over the whole study period for the nuclear $^{14}CO_2$ emissions (see section 3.3.2). The green line (bottom) represent the ffCO_2 equivalent theoretical corrections that need to be applied over the whole study period for heterotrophic respiration from the biosphere (see section 3.3.1). The black points represent times flask samples were taken and therefore the corrections that were applied to each flask measurement.

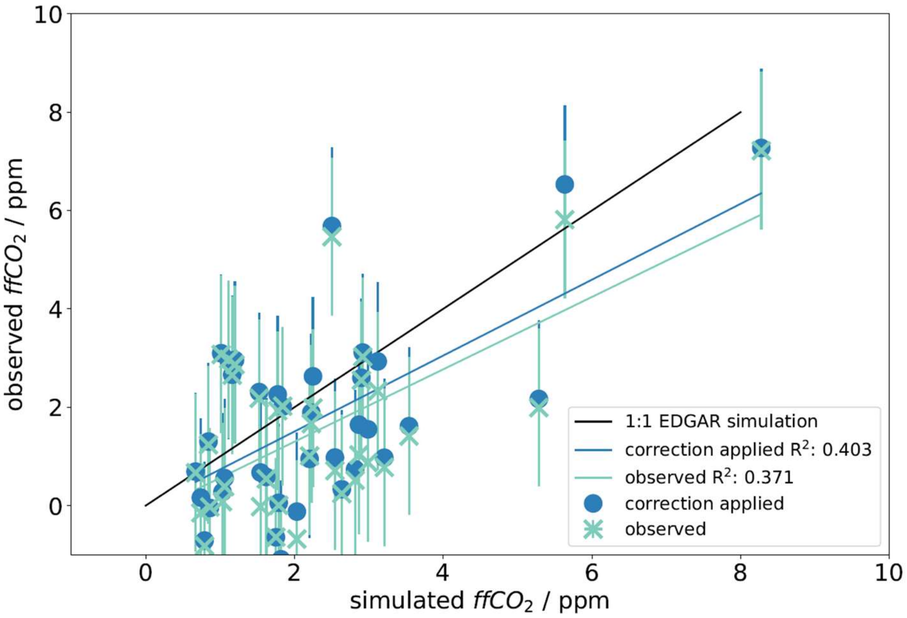

Figure 4. Comparison of fossil fuel CO_2 (observed $ffCO_2$) derived from $\Delta^{14}CO_2$ measurements made at TAC (section 3.3, Equation 4), compared to simulated $ffCO_2$. The simulated $ffCO_2$ was calculated from NAME model back trajectories and the EDGAR 2010 fossil fuel emission inventory according to section 3.1. Observations that have been corrected for nuclear (section 3.3.2) and biospheric (section 3.3.1) influence are shown as blue points, whereas the uncorrected values are shown as green crosses. The 1:1 line shown in black represents the theoretical line where observed data matches the simulated values and therefore the emission inventory exactly. The linear regression lines for the comparison of the modelled $ffCO_2$ to the corrected and uncorrected observed $ffCO_2$ are shown as blue and green lines, respectively. Error bars = 1.8 ppm.

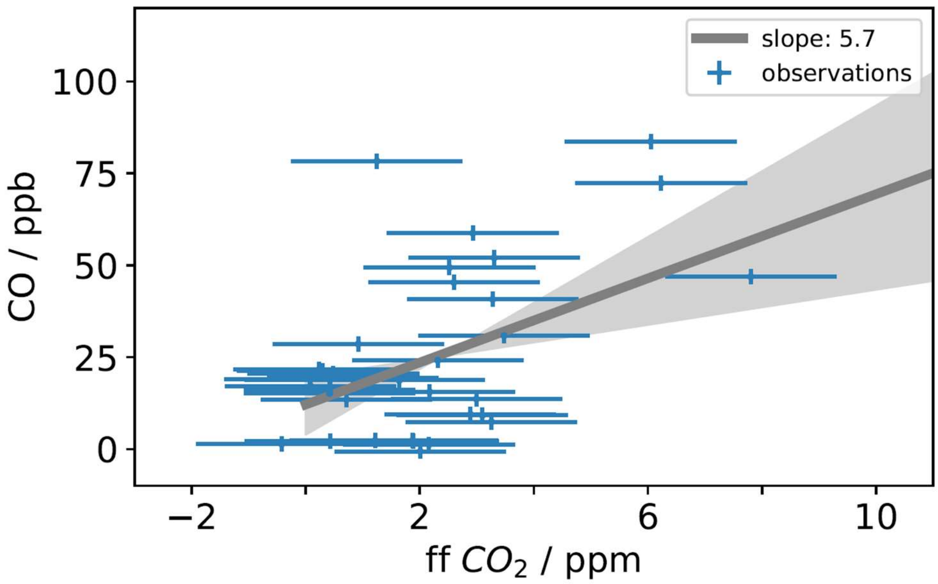

660 **Figure 5. This figure shows the CO enhancement CO_{enh} at TAC (Section 4.2.3) against the observed $ffCO_2$ derived from $\Delta^{14}CO_2$ measurements. The slope of the linear regression is used to calculate the CO_{enh}/ $ffCO_2$ ratio at TAC. The grey line shows the linear regression and grey shading shows the 5-95 % uncertainty estimate of the linear regression. Results of the linear regression calculation of different subsets of this dataset can be found in table 2.**

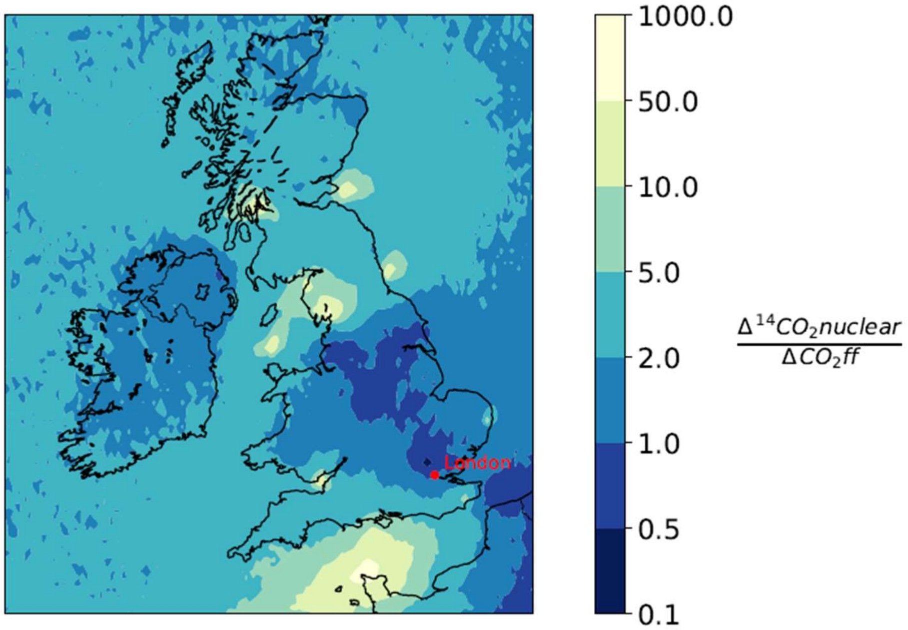

665

Figure 6. This figure shows the ratio of modelled $^{14}CO_2$ nuclear values ($^{14}CO_2$ nuclear) to modelled fossil fuel CO_2 values (CO_2ff) in the UK. The values represent yearly averages, calculated with a 1 year (June 2012 - June 2013) forward run performed in NAME. CO was used as a proxy for $ffCO_2$ and the conversion factor 5.7 ppb ppm^{-1} was used to convert CO to CO_2 (see section 5). High values in yellow represent regions with a large influence from nuclear $^{14}CO_2$ emissions, compared to the fossil fuel emissions. Whereas darker blue areas with a lower $^{14}CO_2$/$ffCO_2$ ratio represent areas where the influence from fossil fuel emissions on $\Delta^{14}CO_2$ is larger than the influence from nuclear emissions.